Available online at www.sciencedirect.com
SCIENCE DIRECT®
Journal of Solid State Chemistry 177 (2004) 2177–2182
JOURNAL OF SOLID STATE CHEMISTRY
http://elsevier.com/locate/jssc

Electron diffraction evidence for continuously variable, composition-dependent O/F ordering in the ReO_3 type, $Nb^{V}_{1-x}Nb^{IV}_{x}O_{2-x}F_{1+x}$, $0 \leqslant x \leqslant 0.48$, solid solution

Frank J. Brink,[1] Lasse Norén, and Ray L. Withers*

Research School of Chemistry, Australian National University, Science Road, GPO Box 4, Canberra ACT 0200, Australia

Received 22 October 2003; received in revised form 27 January 2004; accepted 2 March 2004

Abstract

A spread of compositions within the $Nb^{V}_{1-x}Nb^{IV}_{x}O_{2-x}F_{1+x}$ solid solution have been successfully synthesized in the range $0 \leqslant x \leqslant 0.48$. In each case electron diffraction has revealed the presence of strong planar diffuse scattering perpendicular to each of the three $\langle 001 \rangle$ directions at the $\mathbf{G} \pm \langle hkq \rangle^*$ regions of reciprocal space, where $\mathbf{G}$ represents a Bragg reflection of the ReO_3 type average structure, h and k are continuously variable and q is a fixed (at any one particular composition), composition-dependent parameter in the range from 1/3 to 1/2. Careful electron probe microanalysis indicates that the value of q is directly related to composition via the equation $q = (x+1)/3$ and hence acts as a "chemical ruler" for the composition. A plausible model for the implied one-dimensional O/F ordering as well as for the observed shift in the position of the diffuse versus composition is provided via a crenel type occupational atomic modulation function.

Keywords: Diffuse scattering; Oxygen flourine ordering

1. Introduction

Crystallographic investigations of many oxyfluoride systems, whether line phases or solid solutions, have almost invariably reported a statistical distribution of O^{2-} and F^- ions at the anion site positions. This is despite the fact that bond valence sum calculations and/or independent spectroscopic evidence [1,2] often strongly suggests that O/F ordering must be occurring, at least on the local scale.

The difficulty in providing solid evidence for O/F ordering can be attributed largely to the similarity in scattering factor of O^{2-} and F^- for X-ray, electron and neutron diffraction making differentiation of these anions difficult. To further complicate matters, O^{2-} and F^- ions scatter very weakly relative to the (generally much heavier) cations for X-rays and electrons which implies that evidence for O/F ordering is always going to be weak when compared to the average structure Bragg reflections and is therefore going to be difficult to detect. An additional complicating factor is that true, long range O/F ordering may not be required to satisfy local bond valence sum requirements, i.e. O/F ordering may not be complete in a full three-dimensional sense [3–5]. In this case, the diffraction evidence for local O/F ordering is not to be found in the average structure Bragg reflections, but rather takes the form of a highly structured diffuse intensity distribution.

A good example of this was found in a recent electron diffraction investigation [5–7] of $Nb^{V}O_2F$, of ReO_3 average structure type (see Fig. 1). This study [5] revealed the presence of characteristic planes of diffuse intensity running through the $\mathbf{G} \pm \langle hk1/3 \rangle^*$ regions of reciprocal space (i.e. perpendicular to each of the major crystal directions a, b and c). The existence of such continuous planes of diffuse intensity, in conjunction with their associated $1/3\langle 001 \rangle^*$ component, implies that O^{2-} and F^- ions are in fact ordered in a characteristic …|O–O–F|–O–O–F… pattern along each of the three $\langle 001 \rangle$ real space directions, albeit without

*Corresponding author. Fax: +61-26-125-0750.
E-mail address: withers@rsc.anu.edu.au (R.L. Withers).
[1] Also at Electron Microscope Unit, Research School of Biological Sciences, Australian National University, Canberra, ACT 0200, Australia.

0022-4596/$ - see front matter © 2004 Published by Elsevier Inc.
doi:10.1016/j.jssc.2004.03.001

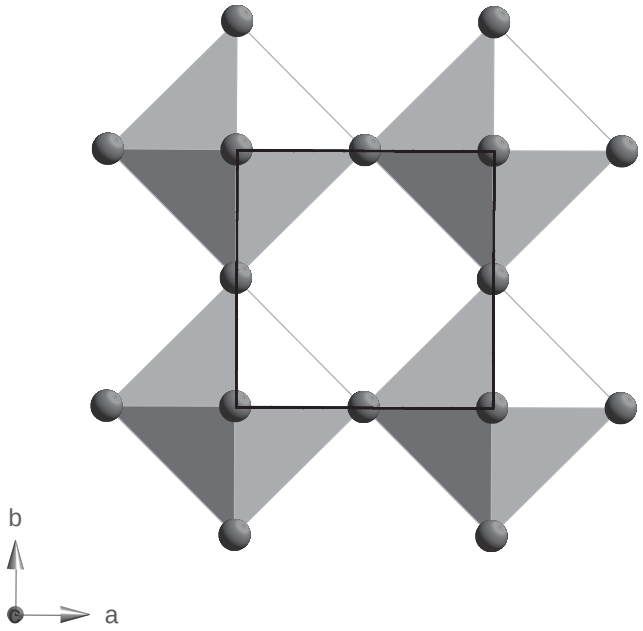

Fig. 1. 3-D projection of the $Nb^{V}_{1-x}Nb^{IV}_{x}O_{2-x}F_{1+x}$, *Re*$O_3$ type average structure. The NbA_6 (A = anion) octahedra are shown shaded. The unit cell is outlined in the center.

there being any correlation from any one such $\langle 001 \rangle$ string to the next. Such an O/F ordering pattern was shown to induce a correlated relaxation of the Nb ions away from the initially over-bonded F^- ions and towards the initially under-bonded O^{2-} ions along each of these $\langle 001 \rangle$ directions. It is these cation shifts which are primarily responsible for the visibility of the observed diffuse distribution.

The correlation of the 1/3 $\langle 001 \rangle^*$ component of the $\mathbf{G} \pm \langle hk1/3 \rangle^*$ sheets of diffuse intensity with the overall anion composition (i.e. the 2:1 O/F ratio) in the case of NbO_2F suggests that the magnitude of this $\langle 001 \rangle^*$ component, q, might be directly correlated to the O/F ratio and hence act as a "chemical ruler" if we could find a way of altering the NbO_2F stoichiometry. A continuous solid solution field has, in fact, been reported in the $Nb^{V}_{1-x}Nb^{IV}_{x}O_{2-x}F_{1+x}$ system all the way from $x = 0$ to 1 [8,9]. It was therefore decided to investigate this solid solution field to see how the highly structured diffuse scattering characteristic of the end-member $x = 0$ composition evolved as a function of stoichiometry.

2. Experimental

2.1. Synthesis

The compounds NbO_2F and TaO_2F were synthesized by dissolving the metal in aqueous HF (48%) and evaporating to dryness, a method first proposed by Frevel and Rinn [10]. However, since the reaction was very sluggish, especially for the Ta, H_2O_2 (*aq*) was added to the mixture, which greatly decreased the overall reaction time. The resultant dry powder was heated in air at 240°C for a few hours and then stored in a glove box under argon.

The synthesis of $NbOF_2$ was attempted by mixing stoichiometric amounts of pre-made NbO_2 (reduced from Nb_2O_5 (Koch-Light Laboratories Ltd., >3N) with H_2 (g) overnight at 800°C), NbF_5 (Aldrich, 98%) and Nb (Apache Chemicals Ltd., 3N3). All reactants were manipulated and mixed in a glove box under an Ar atmosphere to minimize contamination with air or water vapor and then placed in sealed Pt tubes. Since the presence of adsorbed water is almost unavoidable in transition metal fluorides [11] and leads to the evolution of HF gas (and hence excess pressure) on heating, the Pt tubes were in turn placed in sealed quartz tubes under air to minimize the pressure gradient over the Pt tube wall. The ampoules were then placed in a furnace at 690°C for 48 h.

If adsorbed water is present in the metal fluoride starting material, heating is known to lead to the loss of an unknown quantity of F in the form of HF gas and a subsequent increase in the relative amount of O in the reaction product. This makes it impossible to predetermine the composition of the product based solely on the known amount of the starting materials. The presence of water in the starting reaction ingredients was therefore investigated by IR-spectroscopy. The NbF_5 sample was thereby found to contain a significant amount of water (see Fig. 2). As dehydration of the hydrated NbF_5 starting material and ab initio synthesis of anhydrous NbF_5 both require exotic apparatus (pure iron vessels and tubing) as well as extreme reaction conditions (HF gas at >800°C), neither of which were

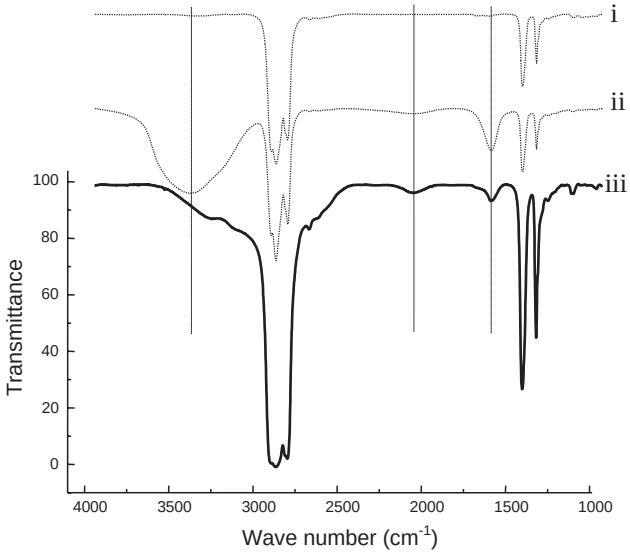

Fig. 2. IR spectra of pure Nujol (i), Nujol with added H_2O (ii) and Nujol with added NbF_5 (iii). The presence of additional water in the NbF_5 is clearly seen (dotted lines).

available to us, the commercially available NbF_5 material had to be used.

As a consequence, it was essential that the true composition of the product (nominal composition '$NbOF_2$') was determined after reaction. This was carried out using Electron Probe Microanalysis (EPMA) (see characterization below). Several compositions within the $Nb^{V}_{1-x}Nb^{IV}_{x}O_{2-x}F_{1+x}$ solid solution were then made by mixing known amounts of NbO_2F and "$NbOF_2$" and reacting these mixtures in sealed Pt-tubes at 690°C for 2 days.

2.2. X-ray powder diffraction (XRD), transmission electron microscopy (TEM) and electron probe micro-analysis (EPMA)

XRD data collected from a Guinier-Hägg camera using Cu$K\alpha_1$ radiation ($\lambda = 1.5406$ Å), were used for phase analysis and to refine unit cell parameters. In the latter case, Si (NBS #640c) was used as an internal standard. Samples suitable for transmission electron microscope (TEM) work were prepared by the dispersion of finely ground material onto a holey carbon film. Electron diffraction patterns (EDPs) were obtained using a Philips 430 TEM.

Electron probe microanalysis (EPMA) was used to determine composition. Samples were prepared by mounting the prepared powders in resin followed by polishing to a <1 μm finish. The analyses were carried out at 15 kV and 1 nA using a JEOL 6400 scanning electron microscope (SEM) equipped with an Oxford Instruments light element EDS detector and Link ISIS SEMquant software as well as a Cameca SX100 using WDS. In order to minimize atomic number, absorption, and fluorescence (ZAF) corrections [12], stoichiometric NbO_2F was used as a calibration standard throughout.

3. Results and discussion

3.1. Electron probe micro-analysis and XRD

Careful EPMA analysis, using end-member $Nb^{V}O_2F$ as a standard, was employed to determine the composition of each of the $Nb^{V}_{1-x}Nb^{IV}_{x}O_{2-x}F_{1+x}$ specimens synthesized. The particle sizes of each of the reaction products were typically in excess of 10 μm, enabling accurate analyses on individual grains in the SEM. The compositional extent of the successfully synthesized $Nb^{V}_{1-x}Nb^{IV}_{x}O_{2-x}F_{1+x}$ compounds was thereby found to range from $0.00(2) \leqslant x \leqslant 0.48(2)$, where 0.48 represents the as measured composition of the synthesis for which the nominal stoichiometry of the starting materials was $NbOF_2$. We do not claim that this necessarily represents the full extent of the solid solution, just that this is the composition range that we were able to prepare using the synthesis procedure described above.

Fig. 3 shows the dependence of the refined ReO_3 type, cubic unit cell a-axis dimension upon composition x, as determined from our combined EPMA and XRD results. Note that the smooth variation in a dimension with composition x appears to obey Vegard's law [13], as indicated by the line of best fit, which has been superimposed (dotted line) on the data (Fig. 3). The cubic unit cell parameter reported for $Nb^{IV}OF_2$ ($x = 1$) by Delobbe et al. [8] has also been included (in brackets) on this plot but deviates significantly from the linear a versus x trend of the data. Our data in fact suggest that the true composition of this phase actually corresponds to an x of ~ 0.62. Given the known problems associated with water in the starting metal fluorides [3,4,11] and the proven need to perform EPMA [4] to determine the true composition of the reaction products, this is perhaps a not entirely surprising result. We note that there is no mention in the earlier work [8] as to whether the composition of the synthesized specimen was determined analytically or simply assumed from the starting composition.

3.2. Electron diffraction

Given the earlier electron diffraction results for the NbO_2F end member [5], electron diffraction has again been used to look for diffraction evidence of O^{2-}/F^{-} ordering within the ReO_3 type average structures of compounds within the $Nb^{V}_{1-x}Nb^{IV}_{x}O_{2-x}F_{1+x}$ solid solution field. Careful tilting experiments show that the reciprocal lattices at all compositions are again characterized by sheets of diffuse intensity, perpendicular to each of the three $\langle 001 \rangle$ directions, at the $\mathbf{G} \pm \langle hkq \rangle^*$ regions of reciprocal space. In any one EDP this gives rise to transverse polarized diffuse streaking running along excited $\langle h0l \rangle^*$ directions of reciprocal space (see for example, Fig. 4). Note that this $\langle h0l \rangle^*$ streaking is generally always observed except at the exact $\langle 001 \rangle$

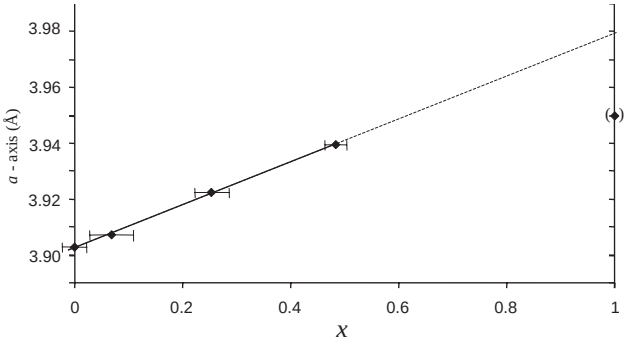

Fig. 3. Plot showing the variation in the average structure unit cell a-axis with composition 'x' in the investigated composition region. The best linear fit is given as a solid line while an extrapolation of the data to cover the whole solid solution is given as a dashed line.

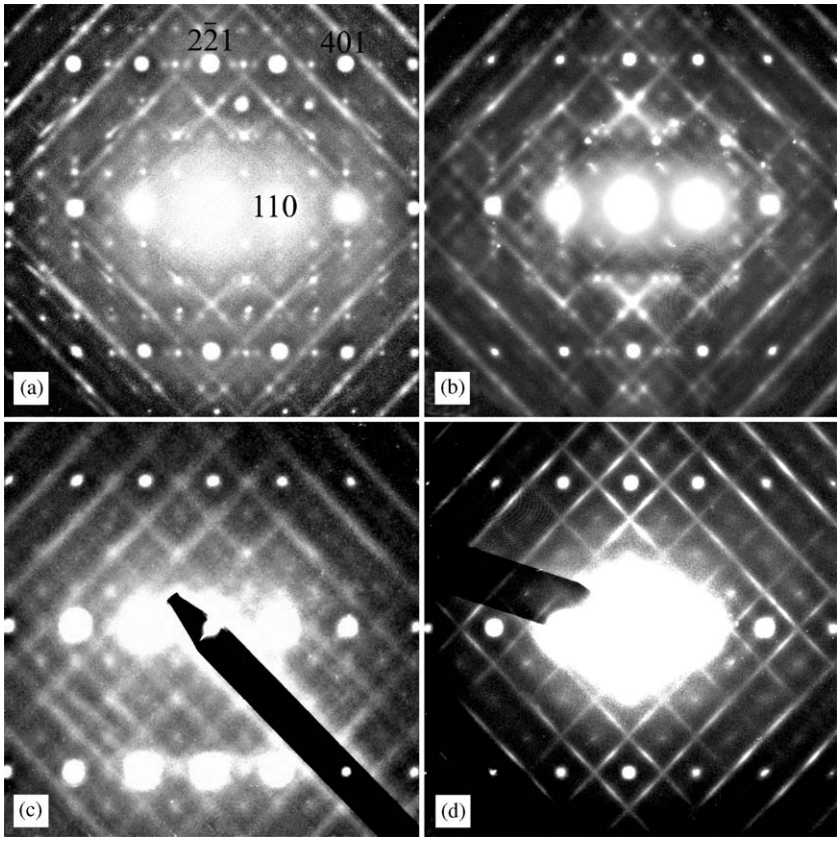

Fig. 4. Typical $\langle 114 \rangle$ zone axis EDPs for (a) the stoichiometric NbO_2F end member composition and the solid solution compositions (b) $NbV0_{.93}Nb^{IV}_{0.07}O_{1.93}F_{1.07}$, (c) $Nb^{V}_{0.75}Nb^{IV}_{0.25}O_{1.75}F_{1.25}$ and (d) $Nb^{V}_{0.52}Nb^{IV}_{0.48}O_{1.52}F_{1.48}$. Note how the position of the diffuse streaking shifts as the O/F ratio is varied.

zone axis orientation where the expected $\langle 100 \rangle^*$ and $\langle 010 \rangle^*$ streaking is systematically absent.

Fig. 4a, for example, shows a $\langle 114 \rangle$ type zone axis EDP for the NbO_2F end member ($x = 0$) composition. The presence of characteristic diffuse streaking at the $\mathbf{G} + \langle hk1/3 \rangle^*$ positions of reciprocal space is clearly visible [5]. At this point it is worth mentioning that an electron diffraction investigation of a synthesized TaO_2F specimen revealed exactly the same strong planar diffuse at the $\mathbf{G} + \langle hk1/3 \rangle^*$ positions of reciprocal space, indicating that TaO_2F is indeed isomorphous to NbO_2F. During a recent investigation on the thermal properties of TaO_2F [14], the authors raised the question as to whether this compound exhibited the same O/F ordering as was observed for NbO_2F.

Figs. 4b, c and d show a further three $\langle 114 \rangle$ zone axis EDPs of synthesized compounds within the $Nb^{V}_{1-x}Nb^{IV}_{x}O_{2-x}F_{1+x}$ solid solution field, at values of $x = 0.07(4)$, 0.25(3) and 0.48(2), respectively. Note that these EDPs are quite reproducible from grain to grain within each of the synthesized compounds. The same transverse polarized sheets of diffuse intensity perpendicular to the three $\langle 001 \rangle^*$ directions of reciprocal space are visible in each case. Careful examination of the diffraction patterns, however, shows that there is a gradual but quite systematic shift of the 1/3 $\langle 001 \rangle^*$ component of the $\mathbf{G} \pm \langle hk1/3 \rangle^*$ sheets of diffuse intensity from $\mathbf{G} + \langle hk1/3 \rangle^*$ ($x = 0$) in Fig. 4a to approximately $\mathbf{G} + \langle hk1/2 \rangle^*$ ($x = 0.48$) in Fig. 4d as the O/F ratio is varied. Thus, the position of these diffuse sheets in reciprocal space can be described more generally by $\mathbf{G} + \langle hkq \rangle^*$, where $q = f(x)$ and $0 \leqslant x \leqslant 1$.

By taking the average of a series of line profiles taken perpendicular to the diffuse streaking as well as through the underlying average structure Bragg reflections for each EDP, it was possible to obtain a more accurate estimate of the position of the diffuse sheets relative to the Bragg positions (see Fig. 5). By correlating this information with the EPMA data it was possible to produce the plot shown in Fig. 6. This graph shows that the position of the diffuse sheets, as defined by the modulation wave vector $\mathbf{q}$ varies, essentially linearly, with composition according to the equation $q = (x + 1)/3$ (superimposed line), making it a very useful and sensitive indicator of composition. In a very real sense q acts as a ''chemical ruler''.

Note that, although the attempted synthesis of $Nb^{IV}OF_2$ was ultimately unsuccessful, extrapolation of the experimental data in Fig. 6 to $x = 1$ predicts diffuse planes should be observed for this compound at the

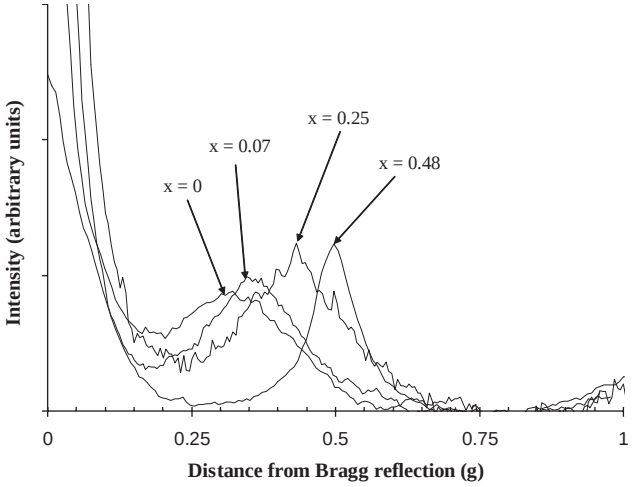

Fig. 5. Line profiles taken perpendicular to the diffuse streaking illustrating the shift in the reciprocal space position of the diffuse with composition.

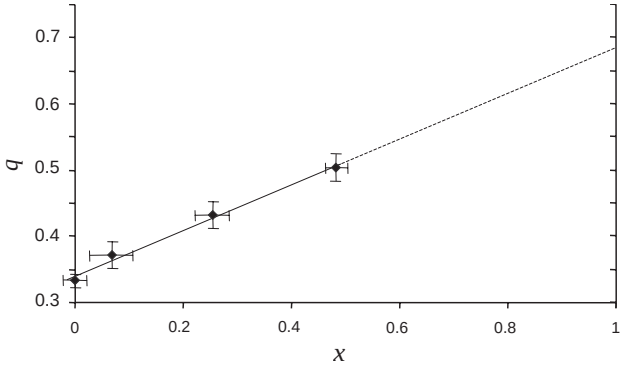

Fig. 6. Graph showing the linear relationship between the **q**-vector for the sheets of diffuse and the composition (x).

$\mathbf{G}+\langle hk2/3\rangle^*$ reciprocal space positions. This is entirely consistent with the earlier prediction that the diffuse sheets for this composition should occur at the $\mathbf{G}-\langle hk1/3\rangle^*$ ($\equiv\mathbf{G}+\langle hk2/3\rangle^*$) positions of reciprocal space.

To model the corresponding real space occupation modulation of the $z\langle 001\rangle$ (z an integer) anion sites along the three $\langle 001\rangle$ directions, a one-dimensional, crenel (square wave) type function [15,16] has been used. Thus, we have assumed that each anion site can only be occupied by either an O or an F, i.e. partial occupancy is not allowed (see Fig. 7). The crenel function is presumed to run (see Fig. 7a) along the x_4 ($\equiv qz$ modulo an integer) axis and contains only two parameters; the crenel width $\Delta=(1+x)/3$ (which defines the F occupation interval) and the crenel midpoint $(1+x)/6$. From the values of x and the primary modulation wave vector $\mathbf{q}=q\langle 001\rangle^*$, it is then possible to predict the sequence of O and F along any $\langle 001\rangle$ string for a given composition. For example, in the case of $Nb^{V}_{0.75}Nb^{IV}_{0.25}O_{1.75}F_{1.25}$ ($x=0.25$) for which

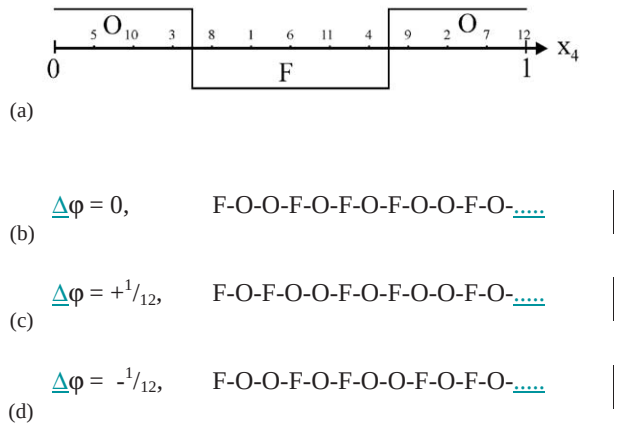

Fig. 7. Diagram showing the Crenel type function used to predict the O/F configurations along the $\langle 001\rangle$ directions for $x=0.25$ in the solid solution $Nb^{V}_{1-x}Nb^{IV}_{x}O_{2-x}F_{1+x}$. The resulting sequence of O and F for each composition can be readily obtained from such an occupational AMF.

$q=1/3$ $(1+x)=5/12$, the $z=12$ repeat sequence …–|F–O–O–F–O–F–O–F–O–O–F–O|–F–O–… is generated by carrying out 12 translations of 5/12 along x_4 (see Fig. 7b).

The absence of any experimentally observed higher order harmonic diffuse sheets, in what should obviously be a square wave like compositional atomic modulation function (AMF), we attribute to the presence of significant phason wobble [17], or random (but limited) shift in the so-called global phase ϕ. This point is illustrated in Figs. 7c and d which show the predicted O–F sequence after introducing an initial global phase shift of $\Delta\phi=+1/12$ and $\Delta\phi=-1/12$ respectively. Note that the predicted composition of anion No. 3 in the string has flipped from O to F and vice versa for anion No. 4 in the case where $\Delta\phi=+1/12$ (see Fig. 7c), while it is the compositions of anions Nos. 8 and 9 which have reversed in the case where $\Delta\phi=-1/12$ (see Fig. 7d). In particular, note that only the anion positions which lie close to the crenel edge in Fig. 7a are affected by a small change in global phase. It is easy to see that if such flipping occurs along an entire $\langle 001\rangle$ column then the effect will be a smearing of the shape of the compositional AMF from square wave to a more sinusoidal shape, leading to a suppression of higher order harmonic diffuse sheets.

In conclusion, it is clear from this investigation that O^{2-} and F^- ions at any composition within the $Nb^{V}_{1-x}Nb^{IV}_{x}O_{2-x}F_{1+x}$, $0\leqslant x\leqslant 0.48$, solid solution region are ordered in one-dimensional strings along each of the major crystal directions a, b and c, albeit with no correlation between strings. The one-dimensional modulation wave vector **q** characteristic of this ordering is shown to vary in a continuous fashion with composition.

References

[1] L.-S. Du, F. Wang, C.P. Grey, J. Solid State Chem. 140 (1998) 285–294.
[2] J. Chappert, J. Portier, Solid State Commun. 4 (1966) 185–188.
[3] F.J. Brink, R.L. Withers, J.G. Thompson, J. Solid State Chem. 155 (2000) 359–365.
[4] F.J. Brink, R.L. Withers, L. Noren, J. Solid State Chem. 161 (2001) 31–37.
[5] F.J. Brink, R.L. Withers, L. Noren, J. Solid State Chem. 166 (2002) 73–80.
[6] B.D. Butler, T.R. Welberry, Acta Crystallogr. A 49 (1993) 736–743.
[7] B.D. Butler, R.L. Withers, T.R. Welberry, Acta Crystallogr. A 48 (1992) 737.
[8] V. Delobbe, J. Chassaing, D. Bizot, Rev. Chim. Miner. 22 (1985) 784–790.
[9] H. Schäfer, D. Bauer, W. Beckmann, R. Gerker, H.G. Nieder-Vahrenholz, K.J. Niehues, H. Scholz, Naturwissenschaften 51 (1964) 241.
[10] L.K. Frevel, H.W. Rinn, Acta Crystallogr. 9 (1956) 626–627.
[11] N.N. Greenwood, A. Earnshaw, Chemistry of the Elements, Reed Educational and Professional Publishing Ltd., Oxford, 1997, p. 820.
[12] M. Love, V.D. Scott, Scanning 4 (1981) 11–130.
[13] A.R. West, Solid State Chemistry and its Applications, Wiley, New York, 1984, p. 366.
[14] J.Z. Tao, A.W. Sleight, J. Solid State Chem. 173 (2003) 45–48.
[15] M. Zakhour-Nakhl, J.B. Claridge, J. Darriet, F. Weill, H.-C. zur Loye, J.M. Perez-Mato, J. Am. Chem. Soc. 122 (2000) 1618–1623.
[16] H.-C. zur Loye, M.D. Smith, K.E. Stitzer, A. El Abed, J. Darriet, MRS Symposium Proceeding, GG 1.4.1., 2001, p. 658.
[17] J.D. Axe, Phys. Rev. B 21 (1980) 4181.